

# SCIENTIFIC REPORTS

OPEN

## Emergence of Topological insulator and Nodal line semi-metal states in $XX'Bi$ ( $X = Na, K, Rb, Cs; X' = Ca, Sr$ )

Chiranjit Mondal<sup>1</sup>, C. K. Barman<sup>2</sup>, Sourabh Kumar<sup>1</sup>, Aftab Alam<sup>2</sup> & Biswarup Pathak<sup>1</sup> 

In this article, we predict the emergence of non-trivial band topology in the family of  $XX'Bi$  compounds having  $P\bar{6}2m$  (# 189) space group. Using first principles calculations within hybrid functional framework, we demonstrate that  $NaSrBi$  and  $NaCaBi$  are strong topological insulator under controlled band engineering. Here, we propose three different ways to engineer the band topology to get a non-trivial order: (i) hydrostatic pressure, (ii) biaxial strain (due to epitaxial mismatch), and (iii) doping. Non-triviality is confirmed by investigating bulk band inversion, topological  $Z_2$  invariant, surface dispersion and spin texture. Interestingly, some of these compounds also show a three dimensional topological nodal line semi-metal (NLS) state in the absence of spin orbit coupling (SOC). In these NLS phases, the closed loop of band degeneracy in the Brillouin zone lie close to the Fermi level. Moreover, a drumhead like flat surface state is observed on projecting the bulk state on the [001] surface. The inclusion of SOC opens up a small band gap making them behave like a topological insulator.

Symmetry protected nontrivial band topology has become an area of paramount research interest for unravelling novel dimensions in condensed matter physics<sup>1,2</sup>. The time reversal invariant topological insulator (TI) has stimulated intense interests due to their intriguing properties, such as gapless boundary states, unconventional spin texture and so on<sup>3-5</sup>. The recent years have witnessed a series of theoretical developments which have enabled us to classify the  $Z_2$ - type non-magnetic band insulators. For example, the  $Z_2$ - even (ordinary) and  $Z_2$ - odd (topological) states are separated by a topological phase transition, where the bulk gap diminishes during the adiabatic deformation between these two states<sup>6</sup>. In two-dimensional (2D) systems,  $Z_2$ - odd class can be distinguished by the odd number of Kramer's pairs of counter propagating helical edge states, whereas in three-dimensional (3D) systems, it can be characterized by the odd number of Fermi loops of the surface band that encloses certain high symmetry points in the Brillouin zones (BZ)<sup>3</sup>. Soon after the experimental realization of quantum spin hall effect in 2D HgTe quantum well<sup>4</sup>, a number of 2D and 3D TI systems have been theoretically predicted and experimentally verified<sup>7-10</sup>. In fact, the search for new TI has been extended to zintl compounds<sup>11,12</sup>, antiperovskites<sup>13</sup>, and heavy fermion f-electron Kondo type of systems<sup>14</sup>.

With the conceptual development in the topological field, research on topological material has been extended from insulators to semimetals and metals<sup>15-17</sup>. In topological semimetals, symmetry protected band crossing or accidental band touching leads to a nontrivial band topology in 3D momentum space. The topological properties of such semimetals mainly depend on the degeneracy of the bands at the crossing/touching point. A zero dimensional band crossing with two and four fold band degeneracy defines the Dirac<sup>15</sup> and Weyl semimetal<sup>16</sup>, respectively, which are quasi-particle counterparts of Dirac and Weyl fermions in high energy physics. Low energy Dirac fermions in condensed matter are essentially protected by time reversal symmetry (TRS), inversion symmetry (IS) and certain crystal symmetry. Quasi-particle Weyl fermion state can be realized by breaking either space inversion or time reversal of crystal<sup>16</sup>. On the contrary, in quantum field theory, Dirac and Weyl fermions are strictly restricted by Lorentz invariance. However, in case of nodal line semimetal (NLS), the conduction and valance band touches along a line to form a one dimensional close loop<sup>17</sup>. The characteristic feature of Dirac semimetal (DS) is a point like Fermi surface (FS) at the crossing point<sup>15</sup>, whereas it is 1D circle for NLS<sup>17</sup>. But for Weyl semimetal (WS), FS forms an arc like surface, instead of closed<sup>16</sup>. Due to the nontrivial FSs, all the topological semimetals show some exotic phenomena, such as quantum magneto-resistance<sup>18</sup>, chiral anomaly<sup>19</sup> etc.

<sup>1</sup>Discipline of Metallurgy Engineering and Materials Science, IIT Indore, Simrol, Indore, 453552, India. <sup>2</sup>Department of Physics, Indian Institute of Technology, Bombay, Powai, Mumbai, 400076, India. Correspondence and requests for materials should be addressed to A.A. (email: [aftab@iitb.ac.in](mailto:aftab@iitb.ac.in)) or B.P. (email: [biswarup@iiti.ac.in](mailto:biswarup@iiti.ac.in))

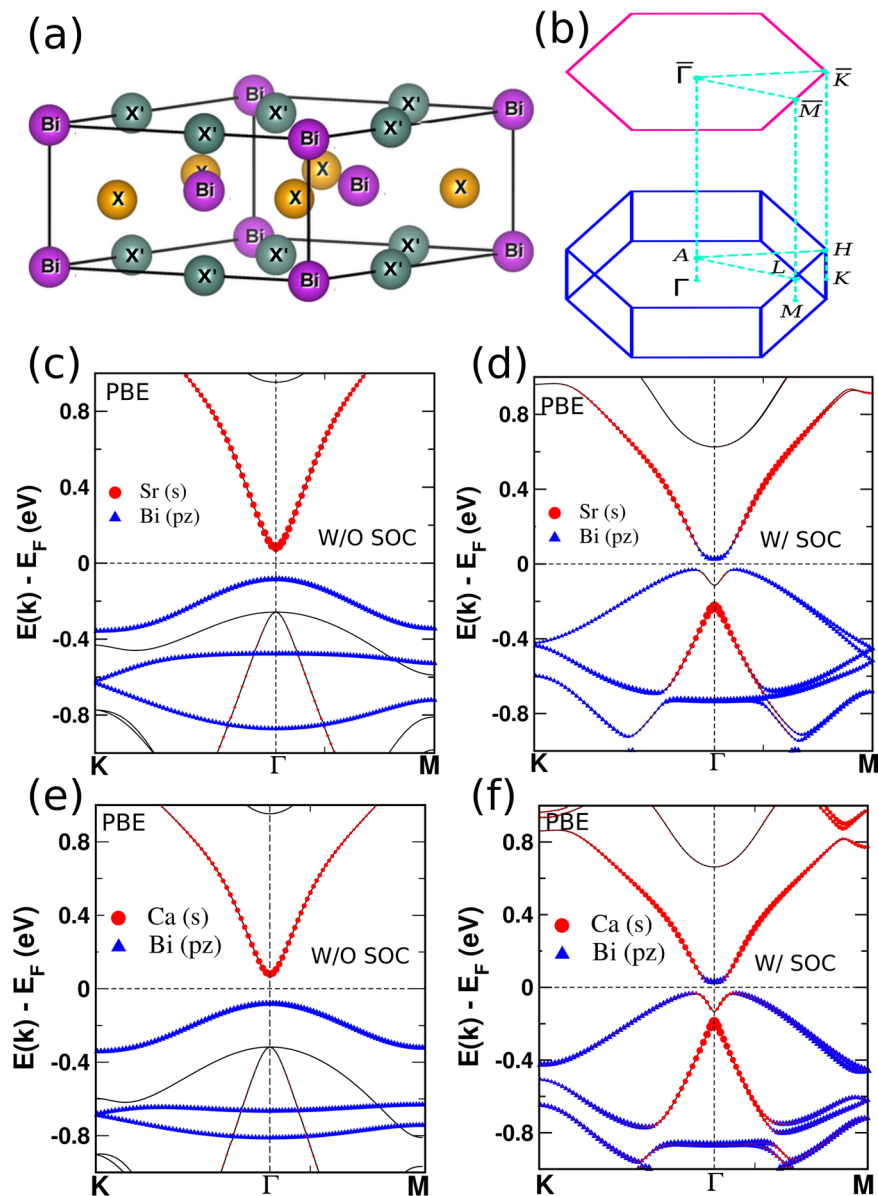


**Figure 1.** (a) Hexagonal crystal structure of  $XX'\text{Bi}$ . (b) Corresponding Brillouin zone (BZ) and two-dimensional BZ projected onto (001) surface. Electronic structures of NaSrBi (c,d) and NaCaBi (e,f) with (W/) and without (W/O) SOC. Red and blue symbols in (c–f) indicate the orbital contributions of Sr/Ca s orbital and Bi  $p_z$  orbital. The sizes of the symbols are proportional to the weightage of the orbitals.

NLS are the precursor states for other topological phases. In general, spinful nodal lines are not robust in the presence of a mass term in Hamiltonian<sup>20</sup>, which can be explained by simple co-dimensional analysis. Thus, inclusion of spin orbit coupling (SOC) can convert the NLS state to DS, WS or TI by opening up a gap around the nodal loop. However, in the presence of an extra crystalline symmetry, nodal line can be robust<sup>20</sup>. Owing to the unique properties such as torus-shaped Fermi surface, relatively higher density of states and interaction induced instability of the FS, NLS can provide a unique playground for the quasi-particle correlations and unusual transport studies<sup>17</sup>.

In this article, we explore the possibility of controlling topological order in a series of ternary compounds  $XX'\text{Bi}$  ( $X = \text{Na, K, Rb, Cs}$  and  $X' = \text{Ca, Sr}$ ). The  $XX'\text{Bi}$  compounds have a non-centrosymmetric hexagonal structure with  $P\bar{6}2m$  (# 189) space group as shown in Fig. 1(a). The theoretically relaxed lattice parameters and formation energy of these systems are provided in supplementary material (SM)<sup>21</sup>. These compounds show interesting topological properties (including NLS state) which can be tuned under various external factors. Recently, NaBaBi has been theoretically studied and predicted to be a topological insulator under hydrostatic pressure<sup>22</sup>.

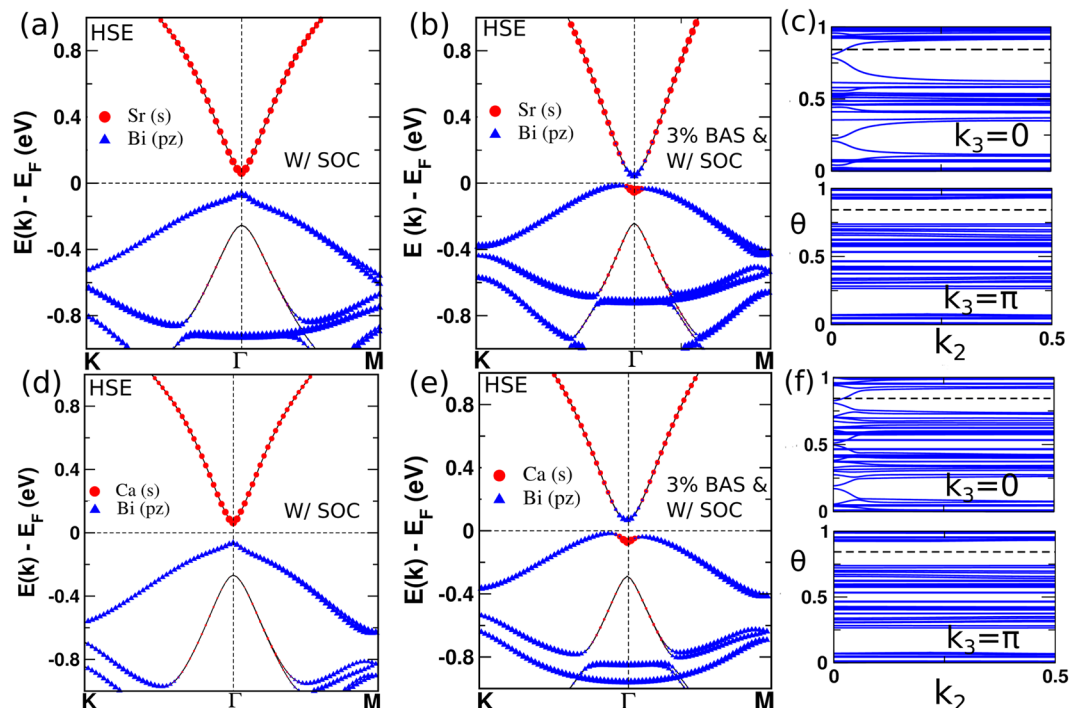


**Figure 2.** Band structures (using HSE06) of (a) pure and (b) 3% biaxially strained NaSrBi. (c) Evolution of wannier charge center along  $k_2$  for NaSrBi. (d–f) Respective plots for NaCaBi.

### Computational Details

All the calculations were carried out using projector augmented wave<sup>23,24</sup> formalism based on Density Functional Theory (DFT) as implemented in the Vienna Ab Initio Simulation Package (VASP)<sup>25</sup>. The Perdew-Burke-Ernzerhof (PBE)<sup>26</sup> type functional with generalized-gradient approximation (GGA)<sup>27</sup> was employed to describe the exchange and correlation effects. All the structures are fully relaxed until the Hellmann - Feynman forces on each atom are less than 0.01 eV/Å and the total energy converge up to  $10^{-6}$  eV. An energy cutoff of 500 eV is used to truncate the plane-wave basis sets for the representation of Kohn - Sham wave functions. The BZ is integrated over  $7 \times 7 \times 11$  gamma centered k-mesh in all the electronic calculations. Hybrid functional (HSE06)<sup>28,29</sup> level of calculations is further carried out to verify the accuracy of PBE-results for electronic structure calculations. Tight-binding (TB) Hamiltonians are constructed using wannier90 package<sup>30</sup> based on the maximally localized Wannier functions<sup>31</sup> (MLWFs). The topological properties including surface spectrum and Fermi surface were analyzed based on the iterative Green's function method<sup>32</sup>. The formation energy and phonon dispersion calculations show that the studied systems are chemically and dynamically stable (Table SI and Figs S1–S3)<sup>21</sup>.

### Topological Insulator

Topological insulating state can be predicted in a material if it shows band inversion driven by spin-orbit coupling<sup>5</sup>. Since the strength of spin-orbit coupling increases with heavy elements, we have systematically studied X-X' elements from group IA-IIA of the periodic table. The electronic structures of all these compounds have been performed using the GGA level of theory. Here, we have mainly discussed NaSrBi and NaCaBi compounds. Our findings related to all other compounds are given in SM<sup>21</sup>. Figure 1(c–f) presents the electronic structures of NaSrBi and NaCaBi compounds. In the absence of SOC, the conduction band minima (CBM) and valence band maxima (VBM) at  $\Gamma$  point are dominated by Sr/Ca  $s$  and Bi  $p_z$  orbital as shown in Fig. 1(c,e). However, inclusion of SOC results in an inverted band order between Sr/Ca  $s$  and Bi  $p_z$  orbitals at  $\Gamma$  point with a direct band gap of  $\sim 80(100)$  meV at  $\Gamma$  point for NaSrBi(NaCaBi) as shown in Fig. 1(d,f) which clearly indicate the non-trivial band topology in these systems.

The non-trivial band topology suggests an interesting surface state<sup>2</sup>. Henceforth, we have studied surface electronic structure of NaSrBi and NaCaBi compounds. Initially, we constructed the slab Hamiltonian from maximally localized wannier functions (MLWF) for Na  $s$ , Ca/Sr  $s$  and Bi  $p$  orbitals. Then we have projected the band structure onto the (001) surface by using the iterative Green's function method as implemented in Wannier-tool<sup>32</sup>. The surface spectra of the slab with a thickness of 200 unit cells are shown in SM (Fig. S4)<sup>21</sup>.

Since the GGA method underestimates the band gap and overestimates the band inversion, we have used the hybrid functional HSE06<sup>28,29</sup> to confirm the predicted non-trivial topology. It turns out that the band inversion between Sr/Ca  $s$  orbital and Bi  $p_z$  orbital disappears at HSE06 level and both of these materials show trivial band order as shown in Fig. 2(a,d). In order to check the evolution of non-trivial band order, we have applied external effects such as pressure, strain and doping. We find that NaSrBi (NaCaBi) system shows a topological insulating behaviour under strain (both hydrostatic as well as biaxial strain induced by epitaxial mismatch). Topological non-trivial properties also emerge in these materials if we partially/fully substitute Na by K, Rb, and Cs in these compounds.

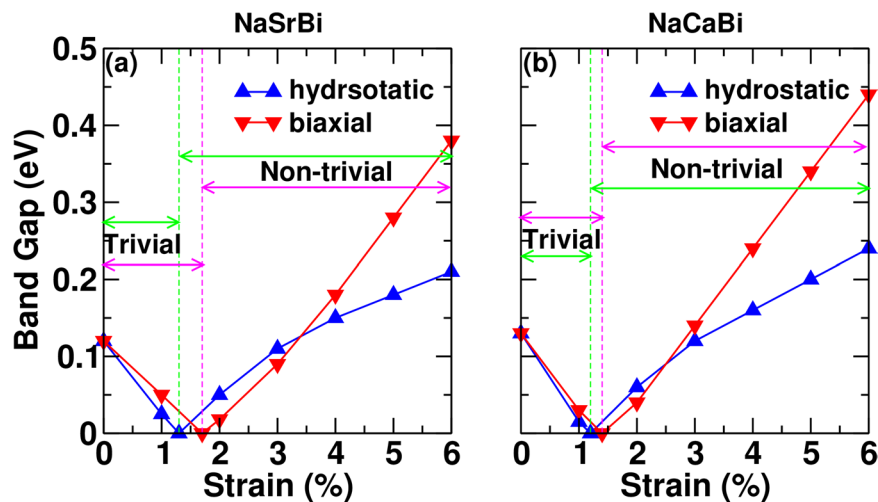


**Figure 3.** Band gap vs. hydrostatic/bi-axial strain(%) for (a) NaSrBi and (b) NaCaBi using HSE06 calculations. Trivial and non-trivial regions for both type of strains are marked by arrowheads.

### Hydrostatic Pressure

We have performed electronic structure calculations on NaSrBi and NaCaBi systems under hydrostatic expansion. A trivial to non-trivial phase transition occurs at  $\sim -2$  GPa ( $\sim 1\%$  expansion in lattice parameter) and both the materials sustain non-trivial band order at higher expansion, as shown in Fig. 3. Since the calculated bulk modulus for NaSrBi and NaCaBi are 21 and 22 GPa respectively, it ensures that such non-trivial band ordering could be realized under low strain. Interestingly, hydrostatic compression also gives non-trivial band ordering (band inversion between Bi-p and Ca/Sr d bands) in these systems. Our calculations show that p-d band inversion can be realized under a large hydrostatic compression (around  $\sim 20$  GPa). The detailed informations of compressive strain and the associated bands are given in SM<sup>21</sup> (Fig. S7). These pressure, however, are quite large and may not be easy to realize. Hence we consider only the hydrostatic expansion and investigated the non-trivial properties of both materials under 3% lattice expansion. Detailed bulk band structure and surface dispersions for both the systems with GGA and HSE06 level are shown in Sec. IV of SM<sup>21</sup>.

### Bi-axial Strain

Next, we have investigated the electronic properties of these materials under biaxial strain (BAS). Experimentally, biaxial strain can be realized by substrate induced lattice mismatch. Accordingly, we have applied biaxial strain along [110] direction to observe the band evolution around the Fermi level. Figure 3 shows the change in the band gap and trivial to non-trivial transform under biaxial strain for NaSrBi and NaCaBi. The trivial and non-trivial regions are mentioned in the plots using arrowheads. Above 1.6% (1.4%) biaxial strain, band inversion occurs in NaSrBi (NaCaBi), which sustains its non-trivial band ordering even at higher strain. Furthermore, we have simulated the bulk band structure for NaSrBi and NaCaBi at +3% biaxial strain as shown in Fig. 2. Figure 2(b,e) clearly shows band inversion between Sr/Ca s and Bi  $p_z$  orbitals at  $\Gamma$  point. To further confirm the topological non-trivialness, we have calculated the topological  $Z_2$  invariant. Owing to the inversion asymmetry in the crystal structure, the parity is not a good quantum number of the Bloch eigenstates. Therefore, parity counting method proposed by Fu and Kane is not applicable here<sup>33</sup>. As such we have adopted the method of Wannier charge center (WCC) evolution in half BZ to calculate the  $Z_2$  invariant along the  $k_2$  direction, as shown in Fig. 2(c,f). It is clear from the figure that the WCC evolution lines cut the reference line one (odd) and zero (even) times in the  $k_3 = 0$  and  $\pi$  planes respectively, for both the systems. Thus the pressure-induced band inversion exhibits a topological phase transition from a trivial insulator to TI.

To see the topological features, we have calculated surface spectra for NaSrBi and NaCaBi at +3% BAS along [110]. The calculated bulk electronic structures using GGA and HSE06 show similar band ordering for both the systems (see Fig. S8 of SM<sup>21</sup>). Hence it is reasonable to expect similar surface dispersion at GGA and HSE06 level of calculations. Therefore, we took the GGA functional to construct the MLWFs and then simulated the surface dispersions for TI phases of two compounds at +3% BAS along [110]. The surface dispersion is shown in Fig. 4. Since the slab calculation involves two surfaces, the corresponding surface bands and spectral intensity maps for both surface (top and bottom) are given.

In the slab model, the top surface is terminated by a X-Bi layer, while the bottom surface is truncated at X'-Bi layer. The asymmetric surface truncation leads to different surface potentials which in turn results into two non-identical Dirac cones lying at different energy as shown in Fig. 4. Another characteristic feature of topological surface state is the helical spin texture. To address this, we have projected the spin directions on the FS of the slab, which is located just above the DP and we find a spin momentum locking feature as shown in Fig. 4. This again confirms the topological non-trivial behavior in both the systems. Similar to most other TI materials, the surface Dirac Cone of both the systems exhibits lefthanded spin texture for top surface states (TSS). The bottom surface states, however, exhibit righthanded spin texture for the Dirac Cone in both the materials.

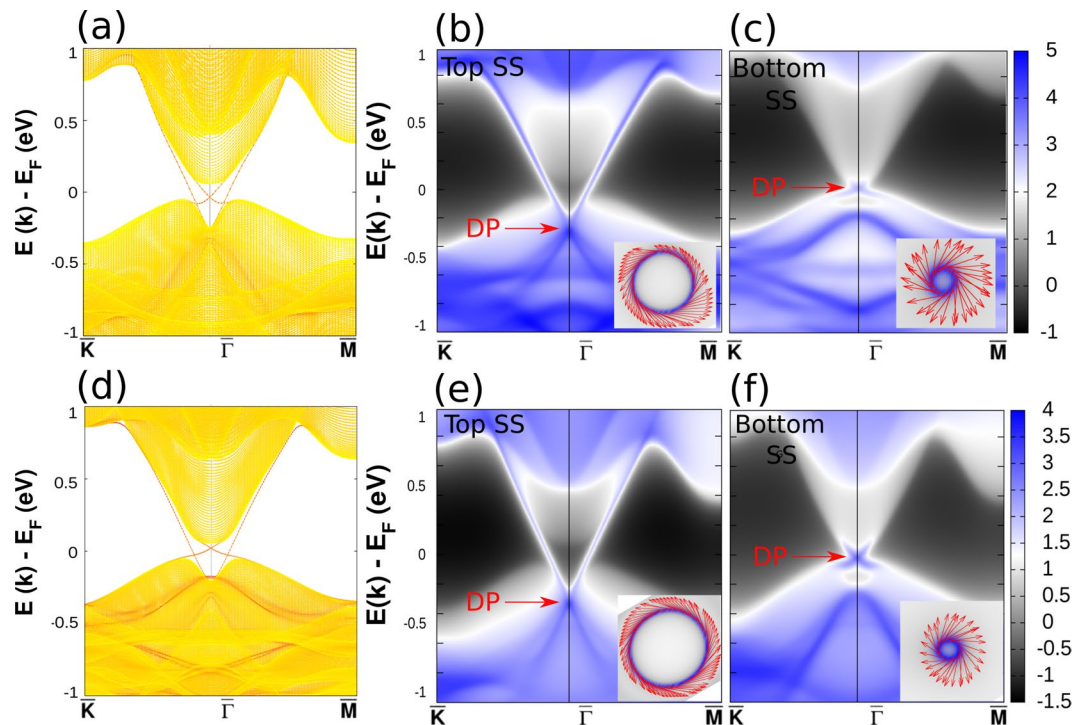


**Figure 4.** (a) Surface dispersion, and surface density of states (SS) for (b) top, and (c) bottom surface layers of NaSrBi under +3% BAS along [110]. (d–f) Respective plots for NaCaBi. The corresponding spin textures around the Fermi energy are shown in their respective insets.

## Doping

Doping or alloying is a promising strategy for hydrostatic expansion/compression of lattice parameters. Therefore, we have doped K, Rb, and Cs at the Na site. Doping with bigger atoms leads to an expansion of lattice parameters, which in turn naturally causes a band inversion instead of a physical hydrostatic expansion imposed on the material. A detailed analysis of such findings, by doping K, Rb or Cs at Na sites in both NaSrBi and NaCaBi are discussed in SM<sup>21</sup> (see Fig. S9).

## Nodal Line Semimetal

In a topological nodal line semi-metal, the bands cross each other due to band inversion and they form a closed loop instead of discrete points around the Fermi level. In contrast to WSs, which have an open arc like FS<sup>16</sup>, NLSs are characterized by the 1D closed ring (a line shape FS) and 2D topological drumhead surface state<sup>17</sup>. The distinguishing characteristic of these drumhead surface state is that they are nearly dispersionless and therefore, have a large density of states near  $E_F$ . Such flat bands and large density of states could provide a potential play ground for the high temperature superconductivity, magnetism, and other related phenomenons.

Here we demonstrate that the materials NaSrBi (NaCaBi) can be transformed into a nodal line semi-metal by complete replacement of Na atom by Rb or Cs. Our detailed calculations predict that the class of systems  $XX'Bi$  ( $X = Rb, Cs$  and  $X' = Ca, Sr$ ) are NLS and show drumhead-like surface flat band. Bulk band structures for all these systems are shown in SM<sup>21</sup> (see Sec. VIII). Of these, we have chosen RbCaBi for detailed analysis here. Figure 5(a,c) shows the band structure of RbCaBi with an inverted band order and 1-D torus like bulk Fermi surface (where conduction and valence band crosses each other along a line) respectively in the absence of SOC. At the  $\Gamma$  point, CBM and VBM have  $A''_2$  and  $A'_1$  representation of  $D_{3h}$ . Along  $\Gamma$ -M, it becomes  $A''$  and  $A'$  representation of  $C_s$ , where as it takes  $B_2$  and  $A_1$  representation of  $C_{2v}$ , along  $\Gamma$ -K, as indicated in Fig. 5(a). The  $D_{3h}$  little group at  $\Gamma$  point ensures the presence of  $\sigma_h$  mirror plane perpendicular to the  $C_3$  principle axis. For spinless case, if two bands belonging from two different irreducible representations (IRs) (here IRs are differed by the eigen value of  $\sigma_h$  symmetry) cross each other in the  $\sigma_h$  plane ( $\sigma_h$  plane contains M,  $\Gamma$  and K high symmetry points in the BZ), then the band hybridization will be prohibited due to the point group symmetry protection. All the crossing points on  $\sigma_h$  plane will have now band degeneracy along a one dimensional loop. Hence the two inter-crossing bands form the nodal loop structure in the BZ. Therefore, in RbCaBi compound the lowest conduction band and highest valence band cross each other along the nodal line and protected from opening up a gap along the nodal loop. Other systems also show similar nature of band structure, confirming the NLS behaviour (see SM Fig. S10)<sup>21</sup>.

From the perspective of bulk boundary correspondence, topologically non-trivial drumhead-like surface states are expected to appear either inside or outside the projected nodal loop on the surface of NLS RbCaBi. In order to calculate the surface states, we have constructed tight binding Hamiltonian using the method of MLWFs and the surface states are projected onto (001) surface using the iterative scheme of Green's function technique. Interestingly, we found a nearly flat surface band which is nestled between two bulk Dirac cones on the (001) surface, as shown in Fig. 5(d,e).

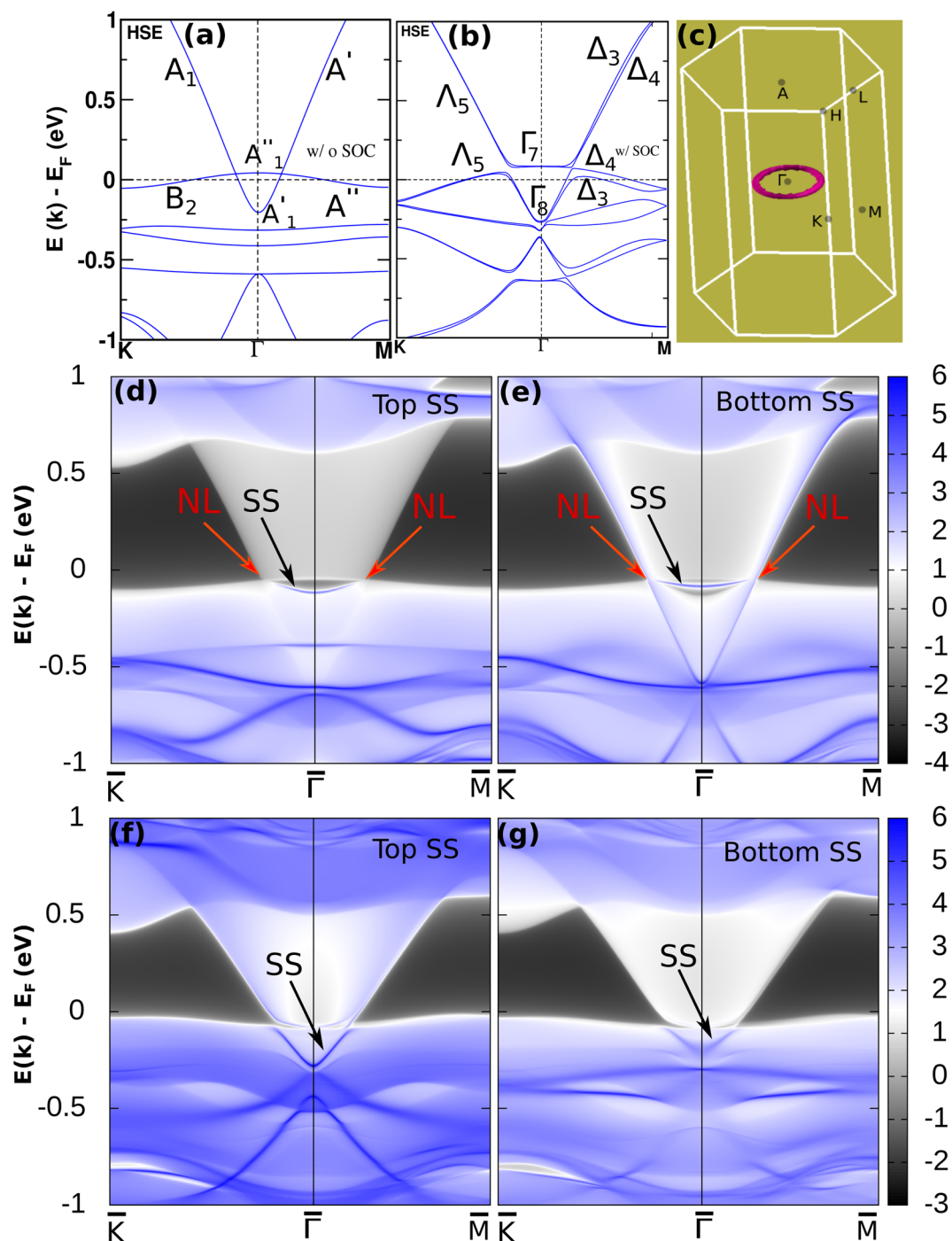


**Figure 5.** (a,b) Bulk electronic structures (using HSE06) of RbCaBi without and with SOC. (c) Shows Fermi surface plot for NLS phase of RbCaBi. (d,e) Are surface density of states (top and bottom) for (001) surface without SOC. (f,g) Are same as (b,c) but with SOC effect.

Further, we take SOC effect into consideration and found that a little gap is opened along the nodal line in the bulk band structure (see Fig. 5(b)). Our first principle calculations show that two set of bands with same IRs  $\Lambda_5$ , which hybridize along  $\Gamma$ -K and open up  $\sim 10$  meV gap at nodal point. However, along  $\Gamma$ -M direction the hybridized gap between the pair of IRs  $\Delta_4$ , is almost zero. Similar gap opening along the nodal line is also observed in several other NLS systems e.g.  $\text{Cu}_3\text{PdN}$  ( $\sim 60$  meV)<sup>34,35</sup>,  $\text{ZrSiS}$  ( $\sim 20$  meV)<sup>36,37</sup>,  $\text{TiB}_2$  ( $\sim 25$  meV)<sup>38,39</sup>,  $\text{CaAgBi}$  ( $\sim 80$  meV)<sup>40</sup>,  $\text{CaPd}$  ( $\sim 27$  meV)<sup>41</sup> and so on. We have also carried out the surface density of states calculation for our material RbCaBi under SOC effect. Indeed we have found drumhead like surface states in (001) surface as shown in Fig. 5(f,g). This, however, is a common feature in almost all the existing NLS compounds<sup>36–39,41,42</sup>, whenever SOC effect is taken into account in any first principles calculation. Even the experimentally reported other NLS systems, such as  $\text{TiB}_2$ ,  $\text{ZrSiS}$ , show somewhat concave surface bands as obtained in our case for RbCaBi

[Fig. 5(f,g)]. As such, we believe that RbCaBi can be a promising candidate for NLS and worthy of careful experimental investigation.

## Conclusion

In summary, using the first principles calculations, we have predicted topologically non-trivial phases including nodal line semi-metal states in a series of compounds belonging to the class of  $XX'Bi$  ( $X = Na, K, Rb, Cs; X' = Ca, Sr$ ). We closely engineer the topology of the bands by applying hydrostatic compression/expansion, bi-axial strain and external doping, which in turn helps to achieve non-trivial band order. Non-triviality is further confirmed by investigating Wannier charge center, surface dispersion and spin texture. NaSrBi and NaCaBi are found to be strong TI under hydrostatic and bi-axial strain. Doping or alloying is another efficient way to control the non-trivial order. Partial or complete replacement of Na by Rb, Cs or K in the compound  $NaX'Bi$  ( $X' = Sr, Ca$ ) helps to intrigue the TI or the NLS phase. We have also studied 1-D bulk Fermi surface and the topological flat surface band properties of systems showing NLS behavior. Possibility of experimental synthesis is confirmed by presenting the chemical stability of all the compounds. We endorse a much higher predictability power of the present report due to the use of HSE06 functionals compared to most of the similar previous reports based on GGA functional. Such accurate ab-initio predictions serve as a guiding path for the discovery of new novel materials.

## References

- Moore, J. E. The birth of topological insulators. *Nature* **464**, 194–198 (2010).
- Hasan, M. Z. & Kane, C. L. Colloquium: Topological insulators. *Rev. Mod. Phys.* **82**, 3045 (2010).
- Kane, C. L. & Mele, E. J.  $Z_2$  Topological Order and the Quantum Spin Hall Effect. *Phys. Rev. Lett.* **95**, 146802 (2005).
- König, M. *et al.* Quantum Spin Hall Insulator State in HgTe Quantum Wells. *Science* **318**, 766–770 (2007).
- Bernevig, B. A., Hughes, T. L. & Zhang, S.-C. Quantum Spin Hall Effect and Topological Phase Transition in HgTe Quantum Wells. *Science* **314**, 1757–1761 (2006).
- Lin, H. *et al.* Half-Heusler ternary compounds as new multifunctional experimental platforms for topological quantum phenomena. *Nature Materials* **9**, 546549 (2010).
- Mondal, C., Kumar, S. & Pathak, B. Topologically protected hybrid states in graphene–stanene–graphene heterojunctions. *J. Mater. Chem. C* **6**, 1920–1925 (2018).
- Xu, Y. *et al.* Large-Gap Quantum Spin Hall Insulators in Tin Films. *Phys. Rev. Lett.* **111**, 136804 (2013).
- Hsieh, D. *et al.* Observation of Time-Reversal-Protected Single-Dirac-Cone Topological-Insulator States in  $Bi_2Te_3$  and  $Sb_2Te_3$ . *Phys. Rev. Lett.* **103**, 146401 (2009).
- Barman, C. K. & Alam, A. Topological phase transition in the ternary half-Heusler alloy ZrIrBi. *Phys. Rev. B* **97**, 075302 (2018).
- Sun, Y. *et al.* Strain-driven onset of nontrivial topological insulating states in Zintl  $Sr_2X$  compounds ( $X = Pb, Sn$ ). *Phys. Rev. B* **84**, 165127 (2011).
- Yan, B., MÜchler, L., Qi, X.-L., Zhang, S.-C. & Felser, C. Topological insulators in filled skutterudites. *Phys. Rev. B* **85**, 165125 (2012).
- Sun, Y., Chen, X.-Q., Yunoki, S., Li, D. & Li, Y. New Family of Three-Dimensional Topological Insulators with Antiperovskite Structure. *Phys. Rev. Lett.* **105**, 216406 (2010).
- Dzero, M., Sun, K., Galitski, V. & Coleman, P. Topological Kondo Insulators. *Phys. Rev. Lett.* **104**, 106408 (2010).
- Liu, Z. K. *et al.* Discovery of a Three-Dimensional Topological Dirac Semimetal,  $Na_3Bi$ . *Science* **343**, 864–867 (2014).
- Xu, Y. *et al.* Discovery of a Weyl fermion semimetal and topological Fermi arcs. *Science* **349**, 613–617 (2015).
- Bian, G. *et al.* Topological nodal-line fermions in spin-orbit metal  $PbTaSe_2$ . *Nat. Commun.* <https://doi.org/10.1038/ncomms10556> (2016).
- Li, H. *et al.* Negative magnetoresistance in Dirac semimetal  $Cd_3As_2$ . *Nat. Commun.* <https://doi.org/10.1038/ncomms10301> (2016).
- Huang, X. *et al.* Observation of the Chiral-Anomaly-Induced Negative Magnetoresistance in 3D Weyl Semimetal TaAs. *Phys. Rev. X* **5**, 031023 (2015).
- Fang, C., Chen, Y., Kee, H.-Y. & Fu, L. Topological nodal line semimetals with and without spin-orbital coupling. *Phys. Rev. B* **92**, 081201(R) (2015).
- See Supplementary material for more details (2018).
- Sun, Y. *et al.* Pressure-induced topological insulator in NaBaBi with right-handed surface spin texture. *Phys. Rev. B* **93**, 205303 (2016).
- Kresse, G. & Joubert, D. From ultrasoft pseudopotentials to the projector augmented-wave method. *Phys. Rev. B* **59**, 1758 (1999).
- Blöchl, P. E. Projector augmented-wave method. *Phys. Rev. B* **50**, 17953 (1994).
- Kresse, G. & Furthmüller, J. Efficient iterative schemes for ab initio total-energy calculations using a plane-wave basis set. *Phys. Rev. B* **54**, 11169–11186 (1996).
- Perdew, J. P. & Zunger, A. Self-interaction correction to density-functional approximations for many-electron systems. *Phys. Rev. B* **23**, 5084–5079 (1981).
- Perdew, J. P., Burke, K. & Ernzerhof, M. Generalized Gradient Approximation Made Simple. *Phys. Rev. Lett.* **77**, 3865 (1997).
- Heyd, J., Scuseria, G. E. & Ernzerhof, M. Hybrid functionals based on a screened Coulomb potential. *J. Chem. Phys.* **118**, 8207 (2003).
- Peralta, J. E., Heyd, J., Scuseria, G. E. & Martin, R. L. Spin-orbit splittings and energy band gaps calculated with the Heyd-Scuseria-Ernzerhof screened hybrid functional. *Phys. Rev. B* **74**, 073101 (2006).
- Mostofi, A. A. *et al.* wannier90: A tool for obtaining maximally-localised Wannier functions. *Comput. Phys. Commun.* **185**, 2309 (2014).
- Marzari, N., Mostofi, A. A., Yates, J. R., Souza, I. & Vanderbilt, D. Maximally localized Wannier functions: Theory and applications. *Rev. Mod. Phys.* **84**, 1419 (2012).
- Wu, Q., Zhang, S., Song, H.-F., Troyer, M. & Soluyanov, A. A. WannierTools: An open-source software package for novel topological materials. *Computer Physics Communications*, <https://doi.org/10.1016/j.cpc.2017.09.033> (2017).
- Fu, L. & Kane, C. L. Topological insulators with inversion symmetry. *Phys. Rev. B* **76**, 045302 (2007).
- Kim, Y., Wieder, B. J., Kane, C. L. & Rappe, A. M. Dirac Line Nodes in Inversion-Symmetric Crystals. *Phys. Rev. Lett.* **115**, 036806 (2015).
- Yu, R. *et al.* Topological Node-Line Semimetal and Dirac Semimetal State in Antiperovskite  $Cu_3PdN$ . *Phys. Rev. Lett.* **115**, 036807 (2015).
- Schoop, L. M. *et al.* Dirac cone protected by non-symmorphic symmetry and three-dimensional Dirac line node in ZrSiS. *Nat. Commun.* **7**, 11696 (2016).
- Neupane, M. *et al.* Observation of topological nodal fermion semimetal phase in ZrSiS. *Phys. Rev. B* **93**, 201104 (2016).
- Liu, Z. *et al.* Experimental Observation of Dirac Nodal Links in Centrosymmetric Semimetal  $TiB_2$ . *Phys. Rev. X* **8**, 031044 (2018).

39. Zhang, X., Yu, Z.-M., Sheng, X.-L., Yang, H. Y. & Yang, S. A. Coexistence of four-band nodal rings and triply degenerate nodal points in centrosymmetric metal diborides. *Phys. Rev. B* **95**, 235116 (2017).
40. Yamakage, A., Yamakawa, Y., Tanaka, Y. & Okamoto, Y. Line-Node Dirac Semimetal and Topological Insulating Phase in Noncentrosymmetric Pnictides CaAgX (X = P, As). *J. Phys. Soc. Jpn.* **85**, 013708 (2016).
41. Liu, G., Jin, L., Dai, X., Chen, G. & Zhang, X. Topological phase with a critical-type nodal line state in intermetallic CaPd. *Phys. Rev. B* **98**, 075157 (2018).
42. Yongping, D. *et al.* CaTe: a new topological node-line and Dirac semimetal. *Npj Quant. Mater.* **2**, 3 (2017).

## Acknowledgements

This work is financially supported by DST SERB (EMR/2015/002057), India. We thank IIT Indore for the lab and computing facilities. C.M., C.K.B. and S.K. thank MHRD for research fellowship. AA acknowledges National Center for Photovoltaic Research and Education (NCPRE), IIT Bombay for possible funding to support this research.

## Author Contributions

All authors potentially contributed to the intellectual contents of this work. C.M. has designed the initial stage of this project. C.M. and C.K.B. have performed all the calculations. S.K. contributed in the technical part of the first principle calculations. The theoretical analysis and discussions were done by C.M., C.K.B., B.P. and A.A. All authors contributed in writing the manuscript. B.P. was responsible for the overall research plan and integration among the different research units.

## Additional Information

**Supplementary information** accompanies this paper at <https://doi.org/10.1038/s41598-018-36869-0>.

**Competing Interests:** The authors declare no competing interests.

**Publisher's note:** Springer Nature remains neutral with regard to jurisdictional claims in published maps and institutional affiliations.



**Open Access** This article is licensed under a Creative Commons Attribution 4.0 International License, which permits use, sharing, adaptation, distribution and reproduction in any medium or format, as long as you give appropriate credit to the original author(s) and the source, provide a link to the Creative Commons license, and indicate if changes were made. The images or other third party material in this article are included in the article's Creative Commons license, unless indicated otherwise in a credit line to the material. If material is not included in the article's Creative Commons license and your intended use is not permitted by statutory regulation or exceeds the permitted use, you will need to obtain permission directly from the copyright holder. To view a copy of this license, visit <http://creativecommons.org/licenses/by/4.0/>.

© The Author(s) 2019